International Journal of Heat and Mass Transfer 52 (2009) 5740–5750

Contents lists available at ScienceDirect

International Journal of Heat and Mass Transfer

journal homepage: www.elsevier.com/locate/ijhmt

Numerical study on high-temperature diluted air combustion for the turbulent jet flame in crossflow using an unsteady flamelet model

K.W. Lee, D.H. Choi *

Department of Mechanical Engineering, Korea Advanced Institute of Science and Technology, Daejeon 305-701, Republic of Korea

ARTICLE INFO

Article history:
Received 22 October 2008
Received in revised form 19 June 2009
Accepted 12 August 2009
Available online 30 September 2009

Keywords:
High temperature air combustion
3D turbulent jet flame
Flamelet model
NO formation

ABSTRACT

The turbulent jet flame in a crossflow with highly preheated diluted air has been numerically investigated. The Favre-averaged Navier–Stokes equations are solved by a finite volume method of SIMPLE type that incorporates the flamelet concept coupled with the standard k–ε turbulence model. The NO formation is estimated by using the Eulerian particle transport equations in a postprocessing mode. For methane and propane with various conditions of inlet air temperature and oxygen concentration, the three-dimensional characteristics of the flame are successfully captured. The jet-flame trajectory is in remarkably good agreement with the existing cold-flow correlations. When the oxygen concentration is high, the maximum flame temperature becomes high and the two fuels show quite different characteristics in the downstream region. On the other hand, for low oxygen concentrations, the temperature difference between the two fuels is relatively small and remains fairly constant throughout the combustion chamber. The propane gives a higher NO formation compared to the methane especially when the oxygen concentration is high. A higher temperature, longer residence time of the combustion gases may be responsible for the higher thermal NO formation.

1. Introduction

The energy and environmental issues have become the prime concern of the industrializing society in recent years, and new combustion technologies that would improve the efficiency and reduce the pollutant emission have evolved. The high temperature diluted air combustion has received much attention because of its potential for energy saving and low nitric oxide emission. Many experimental studies [1–4] showed that the high temperature diluted air combustion is characterized by the very low NO_x emission, low luminosity, high flame stability, large flame volume, and uniform temperature distribution. As for the literature on the computational side [5–7], relatively simple turbulent combustion models such as eddy-break-up model, eddy-dissipation model and PDF/mixture fraction model with equilibrium chemistry have been used. A simple transport equation for nitric oxide concentration with empirical correlations was solved for NO for a given flow and combustion solution.

The turbulent combustion phenomenon in an industrial furnace, however, is too complex to be treated by such simple procedures and a more sophisticated approach is needed to examine the flame structure and control the pollutant formation. Among many combustion models, the laminar flamelet model [8] is proven to be effective in predicting complex physical phenomena by decoupling the chemical reactions from the turbulent flow field. Until recently, most flamelet approaches commonly neglected the unsteady effects, which may become substantial when the process is slow, such as in the formation of NO_x. Pitsch et al. [9] showed that while the steady flamelet model was adequate for the temperature and the species concentration, an unsteady model was needed to improve the prediction of the NO level. Barths et al. [10] proposed a more general Eulerian particle flamelet model (EPFM) that solves a particle transport equation for probability to find the multiple flamelets, and successfully obtained the NO_x and soot formation in a gas turbine combustor. Coelho and Peters [11] evaluated the EPFM extensively for the piloted methane–air jet flame and also applied the model to solve the low oxygen dilution combustion [12]. More recently, Lee and Choi [13] compared two GRI chemical mechanisms, 2.11 and 3.0, on the NO formation using the EPFM.

The primary objective of this study is to extend the laminar flamelet model coupled with the EPFM to three-dimensional cases, and examine the flame structure and NO formation characteristics for the turbulent jet flame in a crossflow of preheated diluted air. The flow is very complex and should be ideal to test the procedure and gain insight into highly three-dimensional combustion phenomena. The effects of the oxygen concentration and different diluents (N_2, CO_2) on combustion characteristics are discussed. Also, the simulations are performed for two different fuels (CH_4, C_3H_8), which have been widely used in industrial fields, to examine the effects of fuel property on the flame characteristics.

* Corresponding author. Tel.: +82 42 350 3018; fax: +82 42 350 3210.
E-mail address: d-h-choi@kaist.ac.kr (D.H. Choi).

0017-9310/$ - see front matter © 2009 Elsevier Ltd. All rights reserved.
doi:10.1016/j.ijheatmasstransfer.2009.08.014

Nomenclature

$a_{p,k}$	Plank mean absorption coefficients for radiating species k
c_p, $c_{p,k}$	specific heat of mixture and species k at constant pressure
D_z	mixture fraction diffusivity
d	jet diameter
h_k	specific enthalpy of species k
I_n	probability of finding nth flamelet
k	turbulence kinetic energy
M_r	momentum flux ratio
P_k	partial pressure of species k
$\dot{q}_{rad}$	radiative heat loss rate per unit volume
r	coordinate in radial direction
t	time
$Sc_{\tilde{Z}}, Sc_{\tilde{Z}''^2}$	Schmidt numbers
T	temperature
T_b	background temperature
u_j	velocity component in jth direction
x_j	coordinate in jth direction
Y_k	mass fraction of species k
Z	mixture fraction
Z''^2	mixture fraction fluctuation
z	vertical distance in the combustor

Greek symbols

χ	scalar dissipation rate
$\tilde{\chi}_{st}$	mean scalar dissipation rate conditioned on stoichiometric mixture
$\hat{\chi}_{st,n}$	surface averaged conditional scalar dissipation rate of nth flamelet
ε	dissipation rate of turbulence kinetic energy
μ_t	turbulent viscosity
ρ	density
σ_B	Stefan–Boltzmann constant
σ_t	turbulent Prandtl number
$\dot{\omega}_k$	chemical production rate of species k
ζ	enthalpy defect

Subscripts

n	nth flamelet particle
st	stoichiometry

Superscripts

$\bar{\phi}$	Reynolds-averaged (density-unweighted) property
$\tilde{\phi}$	Favre-averaged (density-weighted) property

2. Solution procedure

2.1. Flamelet equations

In laminar flamelets, all scalars are functions of the mixture fraction and scalar dissipation rate. Their balance equations for species k and energy for unit Lewis numbers of chemical species are written as

$$\rho\frac{\partial Y_k}{\partial t}-\rho\frac{\chi}{2}\frac{\partial^2 Y_k}{\partial Z^2}-\dot{\omega}_k=0 \tag{1}$$

$$\rho\frac{\partial T}{\partial t}-\rho\frac{\chi}{2}\left[\frac{\partial^2 T}{\partial Z^2}+\frac{1}{c_p}\frac{\partial c_p}{\partial Z}\frac{\partial T}{\partial Z}-\frac{\partial T}{\partial Z}\sum_{k=1}^{N}\left(1-\frac{c_{p,k}}{c_p}\right)\frac{\partial Y_k}{\partial Z}\right]+\frac{1}{c_p}\left(\sum h_k\dot{\omega}_k+\dot{q}_{rad}\right)=0 \tag{2}$$

Here, the scalar dissipation rate is defined as

$$\chi(Z)=2D_Z\left(\frac{\partial Z}{\partial x_j}\right)^2 \tag{3}$$

and Y_k is the mass fraction, T the temperature, ρ the density, c_p the specific heat, h_k the specific enthalpy, $\dot{\omega}_k$ the chemical production rate, D_Z the mixture-fraction diffusivity, and Z the mixture fraction. The radiative heat loss $\dot{q}_{rad}$ is obtained from the optically thin radiation model:

$$\dot{q}_{rad}=4\sigma_B(T^4-T_b^4)\sum P_k a_{p,k} \tag{4}$$

where σ_B is the Stefan–Boltzmann constant and P_k the partial pressure of species k. The Plank mean absorption coefficients $a_{p,k}$ for radiating species k are calculated from the curve fits in TNF workshop (http://www.ca.sandia.gov/TNF/radiation.html). The following one-parameter function proposed by Peters [8] is adopted for the relation between the mixture fraction and the scalar dissipation rate

$$\chi(Z)=\frac{a_s}{\pi}\exp\{-2[erfc^{-1}(2Z)]^2\} \tag{5}$$

where $erfc^{-1}$ is the inverse of the complementary error function and a_s the velocity gradient at the stagnation point. The equation may be rewritten in terms of the stoichiometic values

$$\chi=\chi_{st}f(Z)/f(Z_{st}) \tag{6}$$

where $f(Z)$ represents the exponential term in Eq. (5) and the subscript st denotes the value for the stoichiometric condition.

2.2. Equations for the flow field

The governing equations for the turbulent flow field are the Favre-averaged continuity and Navier–Stokes equations coupled with the standard k–ε model for turbulence closure. A cell centered, colocated finite volume scheme of SIMPLE type is developed and used to solve these equations. The mixing of fuel and oxidizer in the turbulent flow field is described by the transport equations for the mean mixture fraction $\tilde{Z}$ and its variance $\tilde{Z}''^2$

$$\frac{\partial}{\partial t}\left(\bar{\rho}\tilde{Z}\right)+\frac{\partial}{\partial x_j}\left(\bar{\rho}\tilde{u}_j\tilde{Z}\right)=\frac{\partial}{\partial x_j}\left(\frac{\mu_t}{Sc_Z}\frac{\partial\tilde{Z}}{\partial x_j}\right) \tag{7}$$

$$\frac{\partial}{\partial t}\left(\bar{\rho}\tilde{Z}''^2\right)+\frac{\partial}{\partial x_j}\left(\bar{\rho}u_j\tilde{Z}''^2\right)=\frac{\partial}{\partial x_j}\left(\frac{\mu_t}{Sc_{\tilde{Z}''^2}}\frac{\partial\tilde{Z}''^2}{\partial x_j}\right)+2\frac{\mu_t}{Sc_{\tilde{Z}''^2}}\left(\frac{\partial\tilde{Z}}{\partial x_j}\right)^2-\bar{\rho}\tilde{\chi} \tag{8}$$

where the Schmidt numbers $Sc_{\tilde{Z}}$ and $Sc_{\tilde{Z}''^2}$ are chosen to be 0.7 and the mean scalar dissipation rate $\tilde{\chi}$ is modeled as

$$\tilde{\chi}=2.0\frac{\tilde{\varepsilon}}{\tilde{k}}\tilde{Z}''^2 \tag{9}$$

where $\tilde{k}$ is the turbulence kinetic energy and $\tilde{\varepsilon}$ the dissipation rate of $\tilde{k}$.

The mean properties of the reacting mixture in the computational domain are then evaluated by convoluting the tabulated values in the flamelet library with the probability density functions.

$$\tilde{\phi} = \int_{-\infty}^{\infty}\int_{0}^{\infty}\int_{0}^{1} \phi(Z,\chi_{st},\zeta)\tilde{P}(Z,\chi_{st},\zeta)dZ\,d\chi_{st}\,d\zeta \tag{10}$$

where ζ is the enthalpy defect which is the difference between the actual and adiabatic enthalpy. The mean enthalpy defect

$$\tilde{\zeta} = \tilde{h} - [h_o + \tilde{Z}(h_f - h_o)] \tag{11}$$

is obtained from the transport equation for enthalpy by using $\dot{q}_{rad}$ as a source term. Assuming that the mixture fraction and scalar dissipation rate are statistically independent, the probability density function would be constructed as

$$\tilde{P}(Z,\chi_{st},\zeta) = \tilde{P}(Z)\tilde{P}(\chi_{st})\tilde{P}(\zeta) \tag{12}$$

The probability density functions for the mixture fraction and the dissipation rate take, respectively, the forms of the β function and the logarithmic normal distribution while that for the radiation effect is of delta function form. The details are referred to Refs. [8,14] and not repeated here.

2.3. The Eulerian Particle Flamelet Model (EPFM)

The following Eulerian particle transport equations are solved in the postprocessing stage for the species concentrations and NO_x formation:

$$\frac{\partial}{\partial t}(\bar{\rho}\tilde{I}_n) + \frac{\partial}{\partial x_j}(\bar{\rho}\tilde{I}_n\tilde{u}_j) = \frac{\partial}{\partial x_j}\left(\frac{\mu_t}{\sigma_t}\frac{\partial \tilde{I}_n}{\partial x_j}\right) \tag{13}$$

where $\tilde{I}_n(x,t)$ is the probability of finding the nth flamelet at location $\vec{x}$ and time t. Following Barths et al. [10], the initial distribution of the particles in the flow field is prescribed as

$$\tilde{I}_n = \begin{cases} 1 & \text{if } \tilde{Z} > Z_{st} \text{ and } \tilde{T} < 1800\ \text{K} \\ 0 & \text{otherwise} \end{cases} \tag{14}$$

For multiple flamelet particles, the initialization region is divided into the equal number of subregions to which each particle is assigned. The initial probability of finding a flamelet is then equal to unity in its own subregion and zero elsewhere.

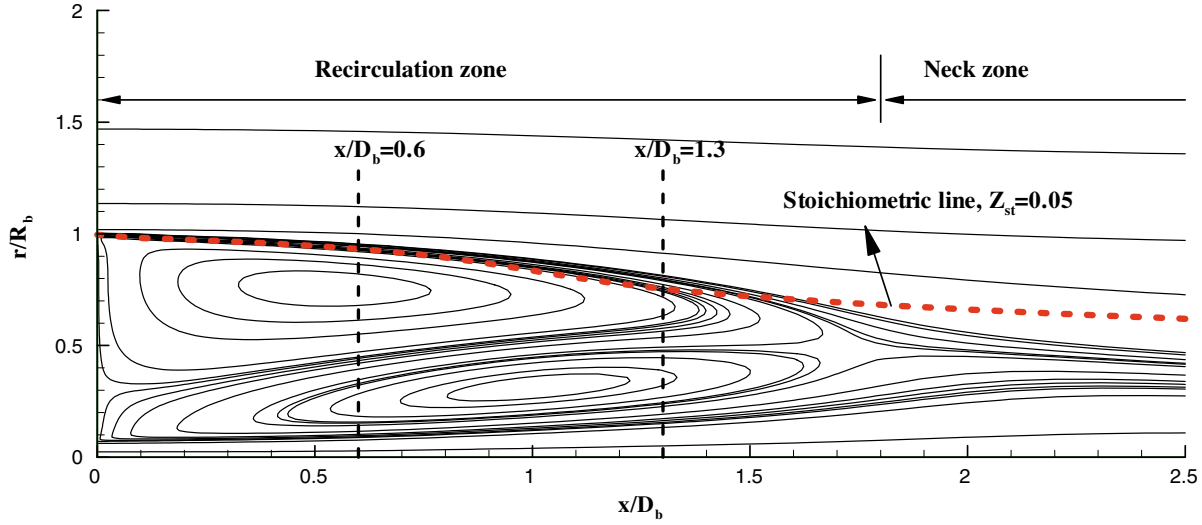

(a) Streamlines near bluff body flame

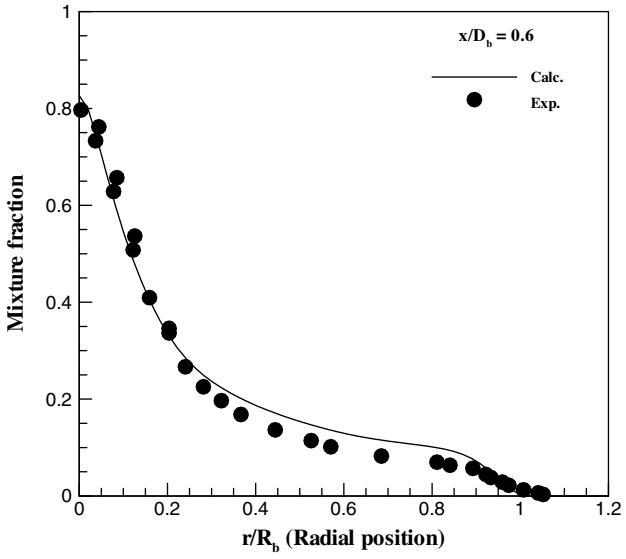

(b) x/D_b=0.6

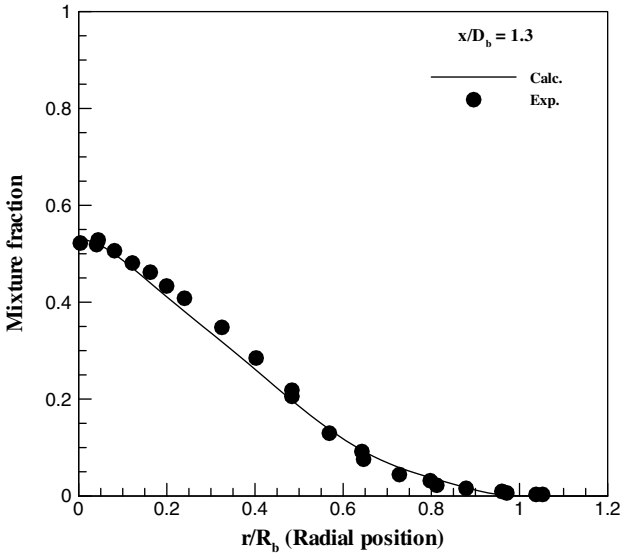

(c) x/D_b=1.3

Fig. 1. Streamlines and mixture fraction profiles at two different axial locations.

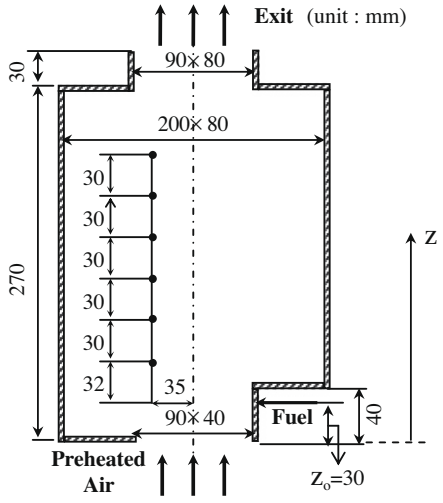

(a) Schematic of experimental setup

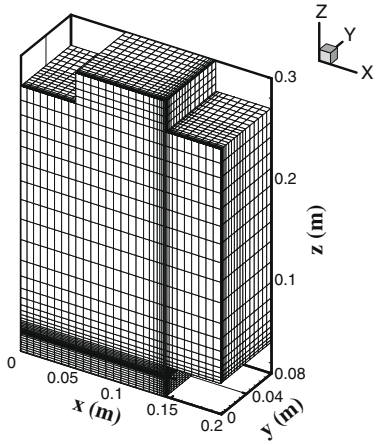

(b) Grid system

Fig. 2. Computational domain of the furnace and grid system.

Flamelet history of each particle is represented as the variation of scalar dissipation rate. The surface averaged conditional scalar dissipation rate is given as

$$\hat{\chi}_{st,n} = \frac{\int_V \tilde{I}_n \bar{\rho} \tilde{\chi}_{st}^{3/2} \widetilde{P}(Z_{st}) dV}{\int_V \tilde{I}_n \bar{\rho} \tilde{\chi}_{st}^{1/2} \widetilde{P}(Z_{st}) dV} \tag{15}$$

where the integration is performed over the whole computational domain. In each subregion, the flamelet equations are solved with $\chi_{st} = \hat{\chi}_{st,n}$. From Eqs. (6) and (9), $\tilde{\chi}_{st}$ can be shown to be

$$\tilde{\chi}_{st} = \frac{2.0 \frac{\tilde{\varepsilon}}{\tilde{k}} \widetilde{Z''^2}}{\int_0^1 f(Z)/f(Z_{st}) \widetilde{P}(Z) dZ} \tag{16}$$

Table 1
Composition of diluted air.

Oxygen concentration (vol%)	Composition of diluted air (vol %)	
	Diluent: N_2	Diluent: CO_2
4	O_2(4):N_2(96)	O_2(4):N_2(15):CO_2(81)
8	O_2(8):N_2(92)	O_2(8):N_2(30):CO_2(62)
10	O_2(10):N_2(90)	O_2(10):N_2(38):CO_2(52)
12	O_2(12):N_2(88)	O_2(12):N_2(45):CO_2(43)
14	O_2(14):N_2(86)	O_2(14):N_2(53):CO_2(33)
16	O_2(16):N_2(84)	O_2(16):N_2(60):CO_2(24)

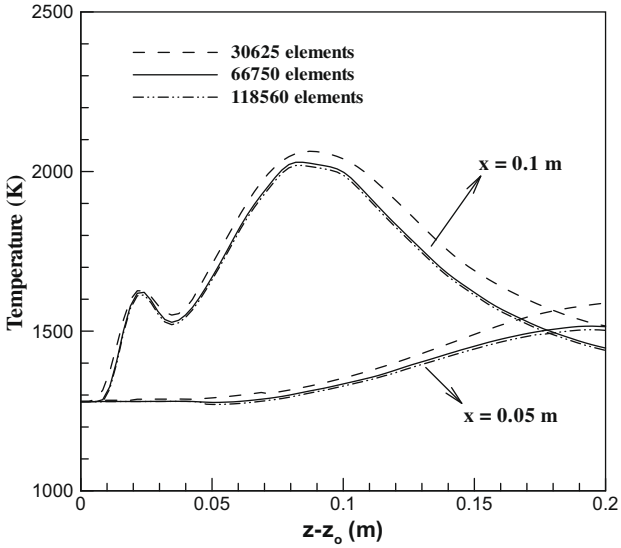

(a) Temperature

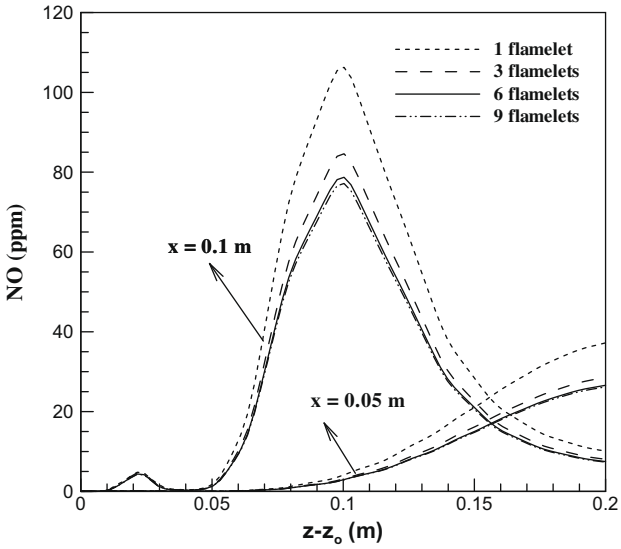

(b) NO concentration

Fig. 3. Effects of grid density and number of flamelet particles for inlet air of 1273 K and 10% O_2 concentration.

The flamelet particles released at time $t = 0$ are dispersed by convection and turbulent diffusion in the combustion chamber. The Favre-averaged mass fractions of chemical species at $\vec{x}$ are calculated by

$$\widetilde{Y}_k(\vec{x}, t) = \frac{\sum_n \int_0^t \widetilde{I}_n(\vec{x}, t') \widetilde{Y}_{k,n}(\vec{x}, t') dt'}{\sum_n \int_0^t \widetilde{I}_n(\vec{x}, t') dt'} \tag{17}$$

This is a weighted average of all flamelet particles over the corresponding period. Here, $\widetilde{Y}_{k,n}(\vec{x}, t')$ is the Favre-averaged mass fraction of species k for the nth flamelet particle:

$$\widetilde{Y}_{k,n}(\vec{x}, t') = \int_0^1 Y_k(Z, \hat{\chi}_{st,n}) \widetilde{P}(Z) dZ \tag{18}$$

where $Y_k(Z, \hat{\chi}_{st,n})$ is the flamelet profile of the unsteady flamelet equations with scalar dissipation rate corresponding to each flamelet history.

Having obtained the steady flamelet solutions, Eqs. 1, 2, 13 with the surface averaged scalar dissipation rates (15) are solved in succession in a coupled manner. The steady-state results are used to

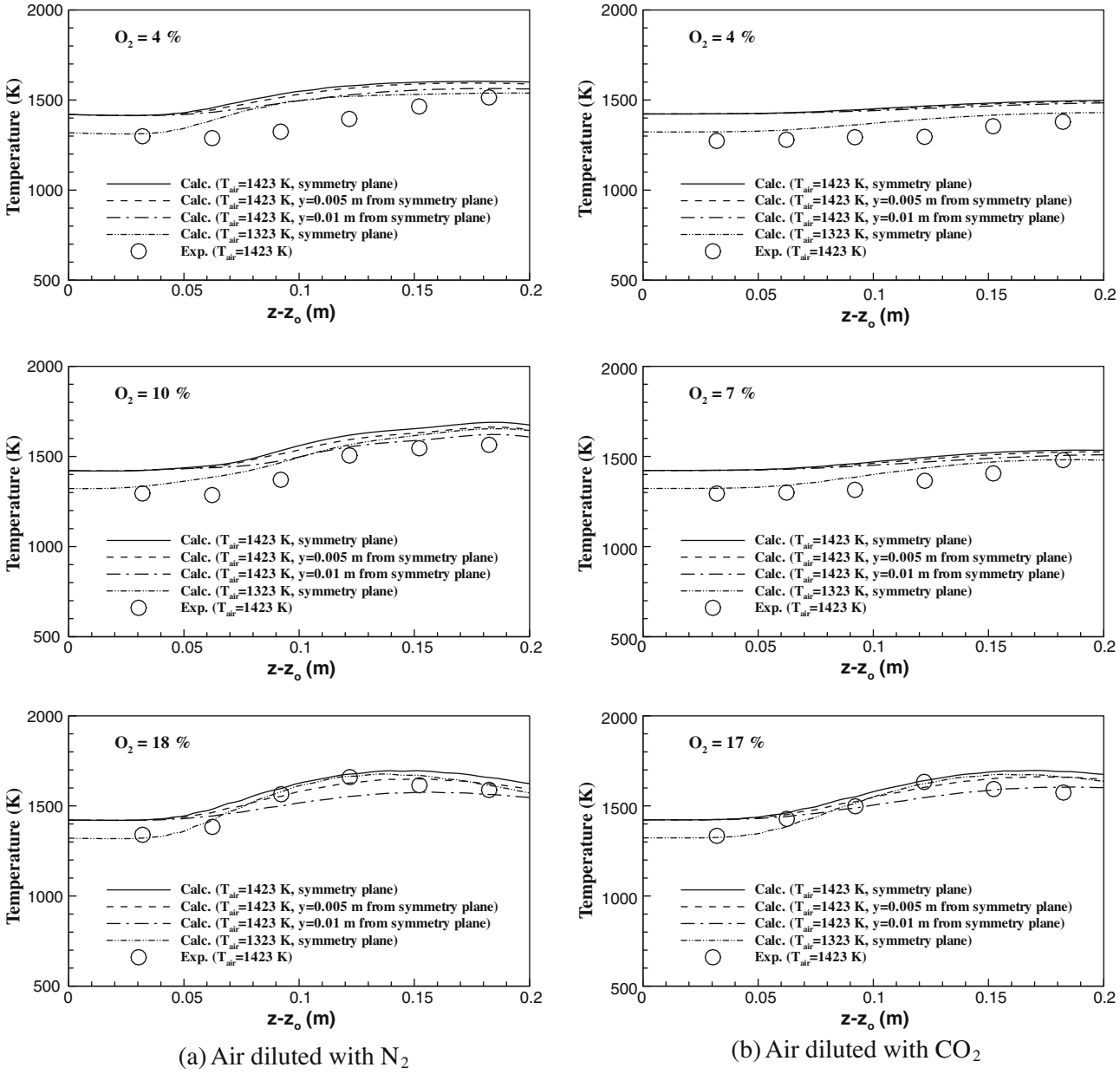

Fig. 4. Temperature distribution in z direction for various O_2 concentrations.

provide the initial condition for this unsteady procedure. The initial mass fraction of species associated with the NO_x mechanism is set equal to zero. The Favre-averaged mass fraction of species k at $\vec{x}$ and t' for the nth flamelet particle is then evaluated from Eq. (18). The calculation is carried out until all flamelet particles are transported away from the combustor. Finally, the species mass fractions $\widetilde{Y}_k$ are obtained from Eq. (17).

3. Results and discussion

Prior to the main simulation, it is proper to mention here that the procedure described in the previous section was thoroughly tested earlier when studying the coaxial jet flame of Fujimori et al. [15]. The computed results for the combustion characteristics including the NO formation, reported in Lee and Choi [16], were in satisfactory agreement with the measured data. The detailed NO formation routes were also discussed in the paper. As another test case, the CH_4/H_2 stabilized bluff-body flame of Dally et al. [17] is considered. The fuel is issued from the nozzle of diameter 3.6 mm, which is surrounded by a solid bluff body of diameter (D_b) 50 mm, with the mean exit velocity of 118 m/s. The velocity of the coflowing air stream is at 40 m/s. The flow field presented in Fig. 1(a) exhibits a pair of strong counter-rotating vortex rings near the base of the bluff body in the recirculation region. The mixture fraction distributions at two different cross-sections compared in Fig. 1(b) and (c) are seen to be in excellent agreement with the measured data. This confirms that the procedure is capable of capturing the combustion characteristics of a highly curved flow in the recirculation region.

Calculations are now extended to a turbulent jet flame in a crossflow to examine the effects of air temperature and oxygen concentrations on the combustion characteristics and NO formation. The flow under consideration is highly three-dimensional and the mixing characteristics are quite different from that of a coaxial jet flame. The fuel jet is issued perpendicular to a uniform air flow through the nozzle at $z = z_0$ as shown in Fig. 2(a). This

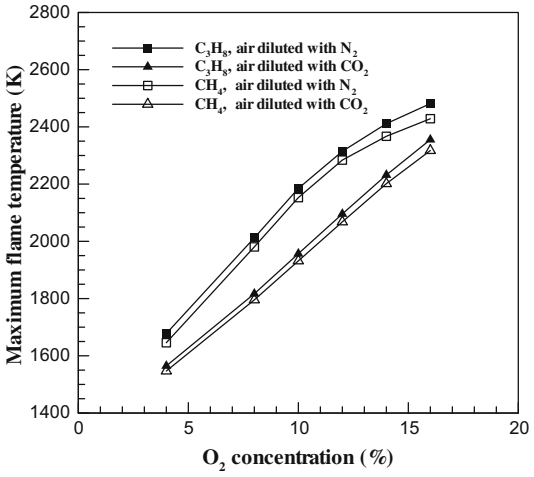

Fig. 5. Maximum flame temperature for two different fuels at inlet air of 1373 K.

enhances the mixing between the fuel and the air. Unlike in the axisymmetric flame, the jet flame in a crossflow exhibits 3D characteristics such as the curved trajectory and recirculation region. Many previous studies on the jet in a crossflow [18–20] have reported that the flow field depends primarily upon the ratio of the jet to the crossflow momentum. It is defined as the square root of the momentum flux ratio:

$$M_r = \left(\frac{\rho_j u_j^2}{\rho_\infty v_\infty^2}\right)^{1/2} \tag{19}$$

where u_j and v_∞ represent the inlet jet and crossflow velocity, ρ_j and ρ_∞ the density of the jet and the crossflow, respectively. The momentum flux ratio varies from 18.4 to 23.9 in the present study due to the change in fuel or oxygen concentration. Also, the jet centerline trajectory was known to be correlated by

$$\frac{x}{M_r d} = A\left(\frac{y}{M_r d}\right)^B \tag{20}$$

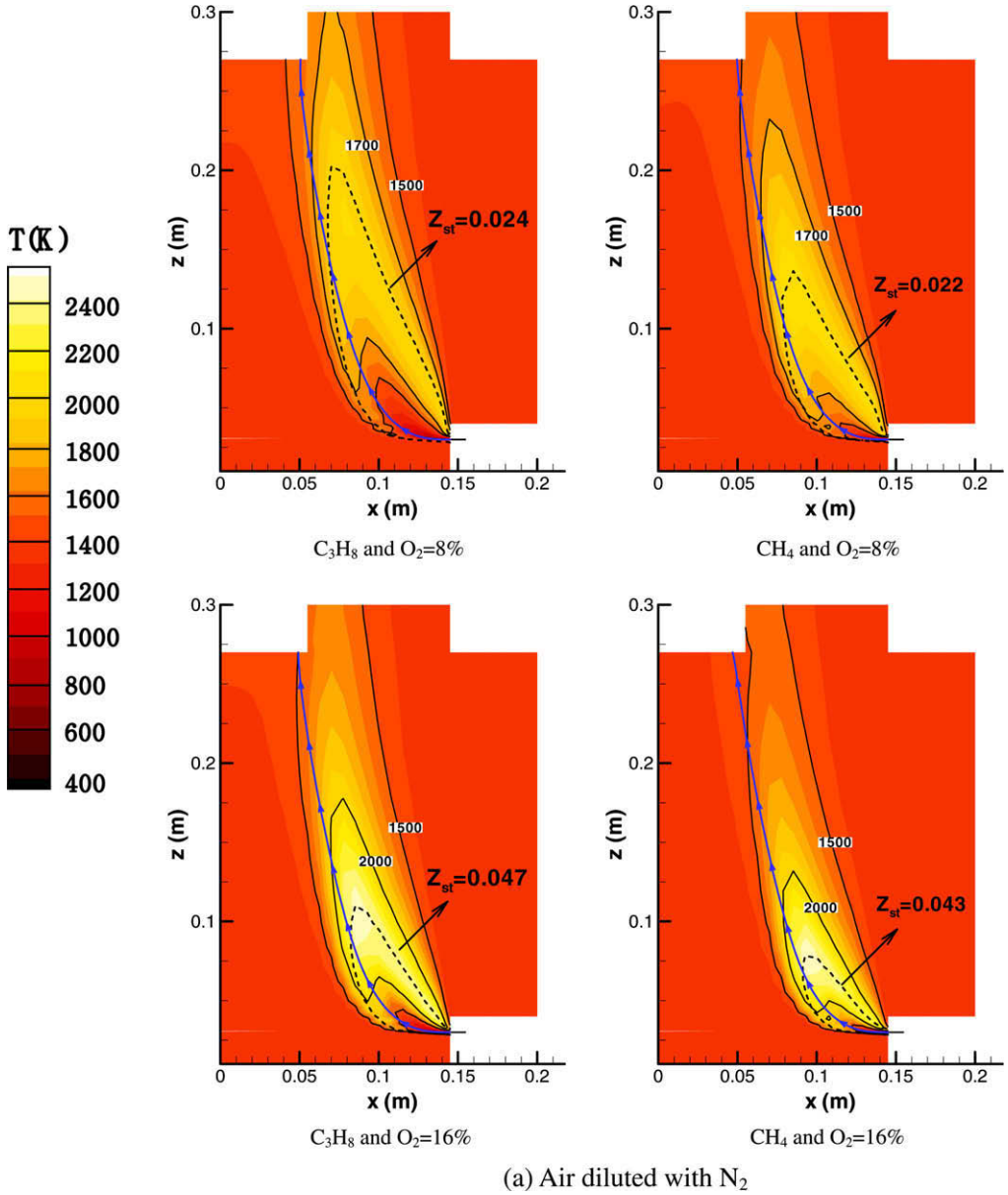

Fig. 6. Temperature fields in the symmetry plane for inlet air of 1373 K.

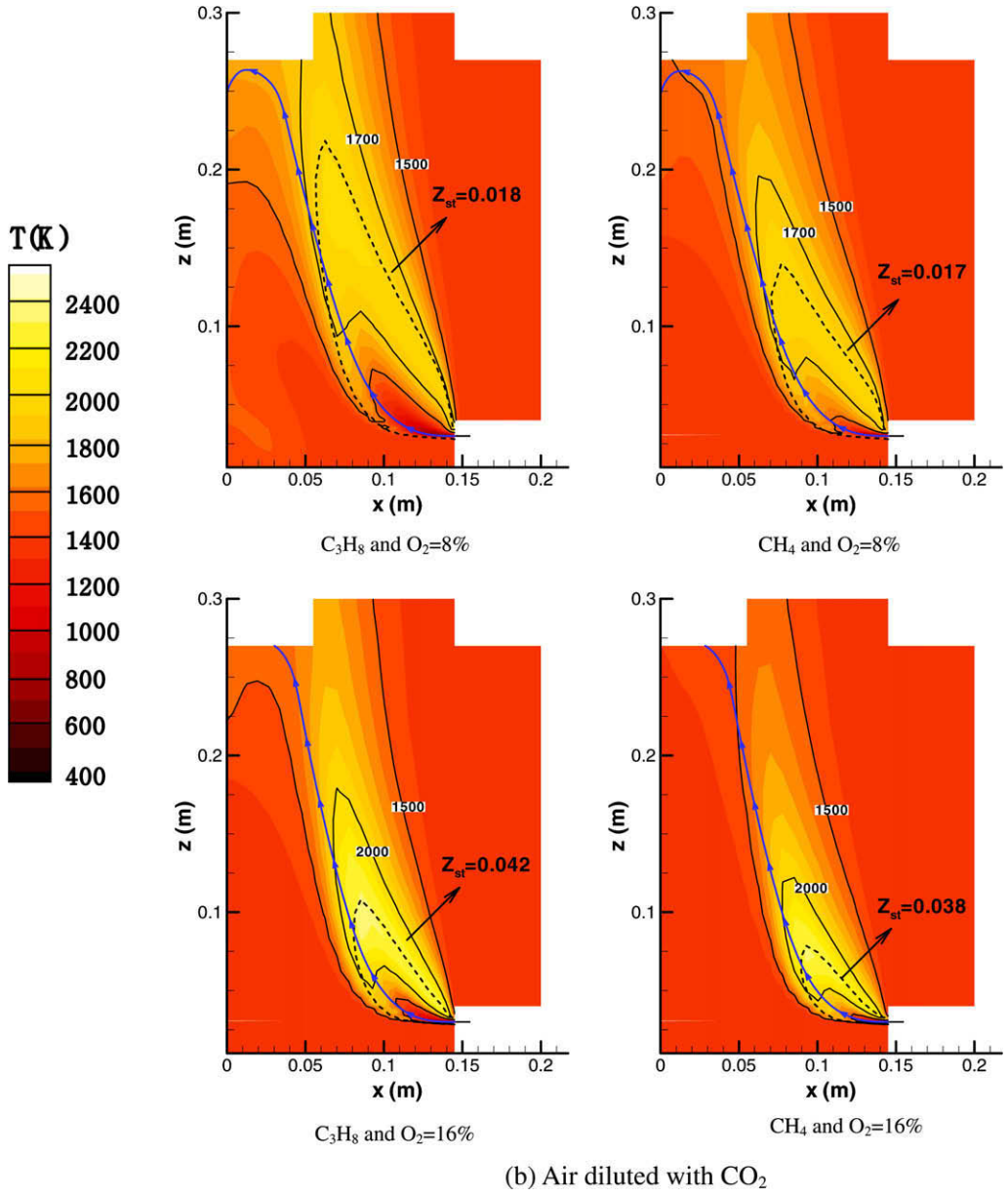

Fig. 6 *(continued)*

where A and B are experimental constants and d the jet diameter. The coordinates x and y denote the directions of the fuel jet and the air flow, respectively.

The present study considers the experimental setup of Hasegawa et al. [1] shown in Fig. 2(a). The propane of 323 K flows at a rate of 2.61×10^{-5} kg/s and the air at 4.88×10^{-3} kg/s. The air temperature is varied between 1273 and 1473 K while its oxygen concentration from 16 to 4 vol% by diluting the air with nitrogen and carbon dioxide. The diluted air composition is given in Table 1. The propane oxidation and the NO_x chemistry are taken from the San Diego mechanism [21] and the skeletal mechanism of Hewson [22]. The CHEMKIN-II and TRANFIT subroutines [23,24] are used to obtain the thermodynamic and transport properties of each chemical species. To examine the effects of the fuel property on combustion characteristics, the methane is also considered besides the propane. To provide the similarity in mixing patterns of two different fuels, the comparison is made for the same jet momentum flux ratio. For the methane oxidation, the GRI 3.0 chemical mechanism is used.

To check the grid resolution, calculations were carried out on three different structured meshes, namely, 30,625, 66,750 and 118,560 elements. The schematic of the domain with the grid is shown in Fig. 2(b) in which the wall is treated as an adiabatic boundary in the calculation. The temperature distributions on the symmetry plane in the vertical direction at two locations $x = 0.05$, 0.1 m are compared in Fig. 3(a). It is observed that the 66,750-element mesh is sufficiently fine to resolve the flow field. The NO concentrations for various number of flamelet particles shown in Fig. 3(b) reveal that six is adequate for unsteady flamelet analysis. Therefore, the mesh of 66,750 elements and six flamelet particles are used in all calculations.

The temperature profiles at the symmetry plane for different oxygen concentrations are compared in Fig. 4. The calculation is seen to overpredict the measured data. The discrepancy was first thought to be due to the uncertainty in measuring stations in the experiment. To clarify the issue, two off-plane ($y = 0.005$, 0.01 m) temperature profiles are also compared in the figure. Although

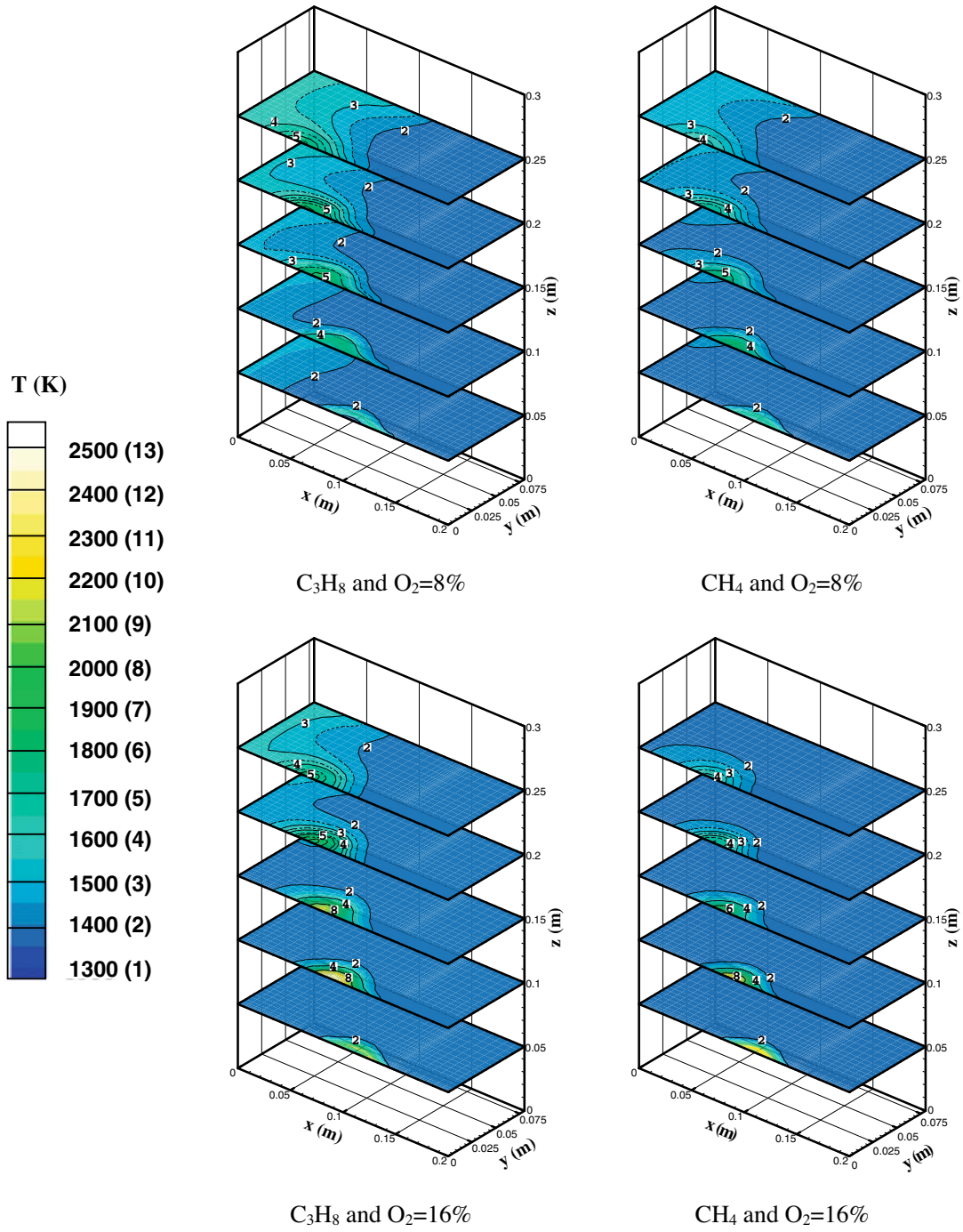

Fig. 7. Cross-sectional temperature fields on various horizontal sections for air diluted with CO_2 at 1373 K.

these give a slightly better agreement in the downstream region, the temperature in the vicinity of the nozzle is still well overpredicted. Among other possibilities, we checked one of the boundary conditions. The inlet air temperature in the experiment was measured outside of the chamber, and thus the air temperature entering the chamber may be lower than 1423 K given in Hasegawa et al. [1]. To examine its effects, the calculation was repeated with a lower inlet temperature, 1323 K, and the results are compared in the figure. It is observed that the results for inlet air of 1323 K are in much better agreement with the experimental data than those for inlet air of 1423 K.

Fig. 5 presents the maximum flame temperature versus the oxygen concentration for two different fuels at inlet air of 1373 K. The maximum temperature increases almost linearly with the oxygen concentration. If the oxygen concentration is lowered from 16% to 4%, the maximum temperature is reduced by about 800 K. This significant drop in temperature is due to the fact that the diluted air makes the flame length longer, and the flame temperature lower and more uniform. The methane gives a slightly lower temperature than the propane. Because of the difference in specific heat of the diluents, the flame temperature is higher when the air is diluted with N_2 than with CO_2 as noted in Yuan and Naruse [5].

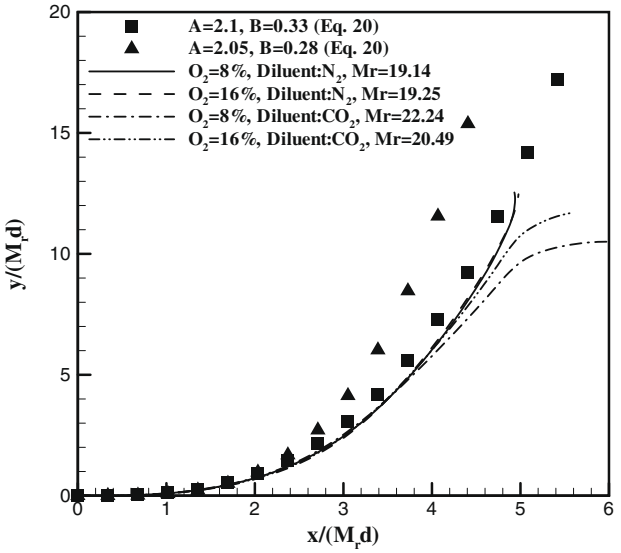

Fig. 8. Centerline jet trajectories normalized by $M_r d$ for propane fuel.

Fig. 6 shows the temperature distributions in the symmetry plane for two oxygen concentrations at the inlet air temperature of 1373 K. The stoichiometric mixture fraction lines and the jet trajectories are also indicated in the figure. Compared to the higher oxygen concentration case, the oxygen concentration of 8% makes the temperature field more uniform and extends the stoichiometric mixture-fraction line farther downstream. The jet trajectories for the two fuels appear to be similar if the oxygen concentration remains the same. This suggests that the mixing patterns of the two fuels are nearly the same if the momentum flux ratios are identical. However, the propane gives a longer flame length than the methane. The phenomena can be seen more clearly in a typical cross-sectional plot of the temperature at $z = 0.05$, 0.1, 0.15, 0.2, 0.25 m in Fig. 7 for air diluted with carbon dioxide. For oxygen concentration of 16%, a high temperature region is observed in the vicinity of $z = 0.1$ m. This region is tempered noticeably if the oxygen concentration is reduced to 8%, and the temperature variation from upstream to downstream becomes small. The propane is seen to give a more uniform temperature distribution especially in the downstream region than the methane.

The jet centerline trajectory for propane is compared in Fig. 8 with the experimental correlation, Eq. (20), with two constant sets. Considering the fact that the correlation is based on non-reacting cold flows, the present results are in remarkably good agreement with Eq. (20) for $A = 2.1$ and $B = 0.33$. The discrepancy observed in the downstream region may be attributed to the confined environment of the furnace coupled with the property changes along the flow direction due to combustion.

The characteristics of temperature distributions in the furnace may be better illustrated in Figs. 9 and 10. Here, T_{max} and T_{mean} denote, respectively, the maximum and average flame temperature in each horizontal cross-section. For two higher oxygen concentrations, i.e., 10% and 16%, the measured flame temperature shown in Fig. 9 reaches its peak before decreases monotonically after that point. Between the two fuels, the methane attains the peak value earlier than the propane but the peak is higher for propane than the other. As the oxygen concentration gets lower, the reduced reaction delays the location of the peak-flame temperature to farther downstream. The difference in the maximum temperature between the methane and the propane reduces as the oxygen concentration decreases. For the lowest oxygen concentration examined, i.e., 4%, the maximum-temperature levels for two fuels

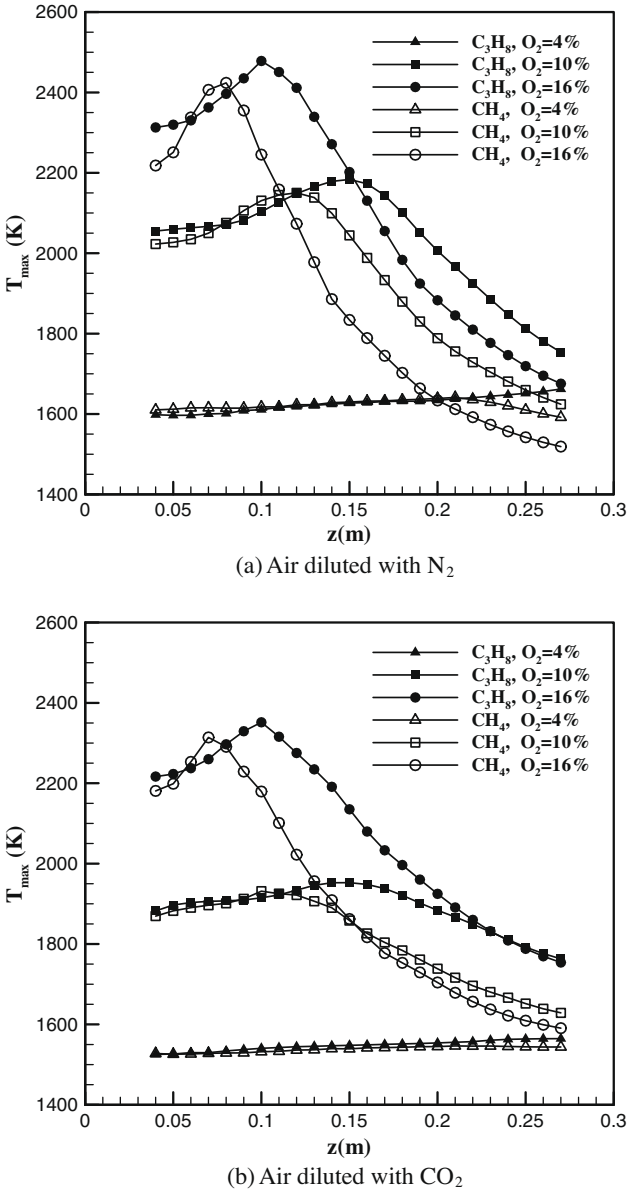

Fig. 9. Maximum flame temperature of horizontal cross-sections along z direction for inlet air of 1373 K.

are nearly identical. The results of the two different diluents show the same trend.

The mean temperature of the horizontal cross-section is shown in Fig. 10. As the oxygen concentration decreases, the mean temperature increases and becomes higher than that of the higher oxygen concentration in the downstream region. This phenomenon is more pronounced in the air diluted with carbon dioxide. This shows that the high temperature diluted air combustion is advantageous as it reduces the maximum flame temperature while keeps the mean temperature level high in the furnace. Although the maximum flame temperature is lower for the air diluted with carbon dioxide than that with nitrogen, the mean temperature is seen to be higher for the air diluted with carbon dioxide particularly in the downstream. The propane gives a higher mean temperature compared to the methane. The difference in the mean temperature between the two fuels is larger for the air diluted with carbon dioxide than that with nitrogen, but it is smaller than 50 K for the same oxygen concentration.

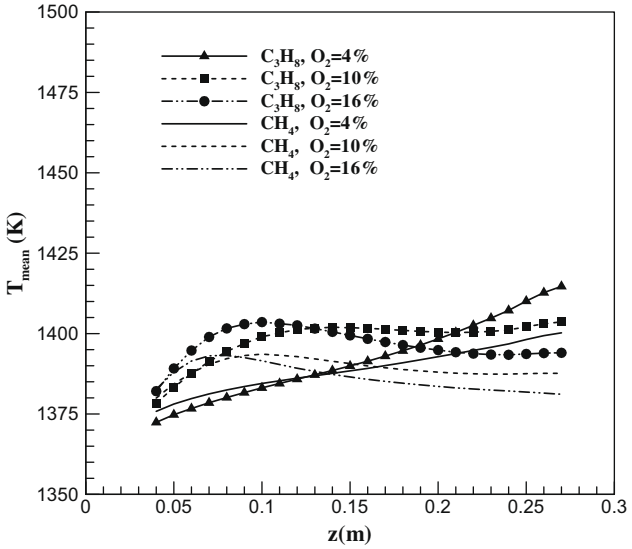

(a) Air diluted with N_2

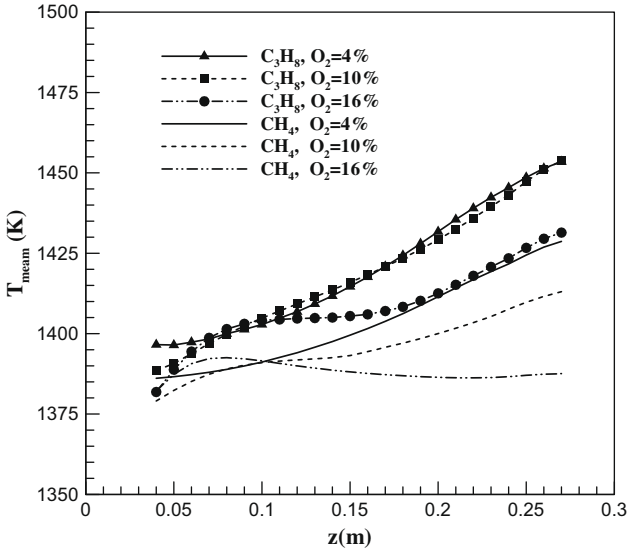

(b) Air diluted with CO_2

Fig. 10. Mean flame temperature of horizontal cross-sections along *z* direction for inlet air of 1373 K.

In Fig. 11, the NO emission indices for the two different fuels are compared for inlet air temperature of 1373 K. The index is defined as the amount of pollutant produced per unit mass of fuel by the combustion process:

$$EINO_x(\mathrm{g/kg}) = \frac{W_{NO_x}\int_V \dot{\omega}_{NO_x}\,dV}{-W_F\int_V \dot{\omega}_F\,dV}\times 10^3 \tag{21}$$

where W_{NO_x} and W_F denote the molecular weights of NO_x and fuel while $\dot{\omega}_{NO_x}$ and $\dot{\omega}_F$ the production rates (mole/m^3 s) of NO_x and fuel, respectively. It is clear from the figure that the lower the oxygen concentration, the lower the NO formation. When the oxygen concentration is less than 10% in the case of air diluted with carbon dioxide, the NO emission indices are fairly low and the difference in the NO emission indices between the two fuels is negligible. When the air is diluted with CO_2, the low amount of nitrogen in the air, which is the main source of the nitric oxide formation, coupled with the low flame temperature seen in Fig. 5, results in a very low NO formation.

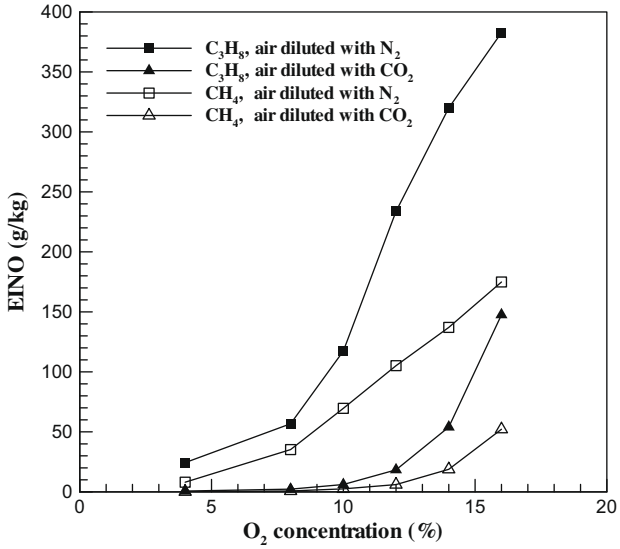

Fig. 11. Emission indices of NO for two different fuels with various oxygen concentrations at inlet air of 1373 K.

As the oxygen concentration increases, however, the NO formation becomes substantial. This is attributed to the thermal NO formation due to the increase in the flame temperature. The difference in NO formation between the two different fuels is seen to increase significantly. It is known that the combustion conditions, such as the flame temperature, oxygen concentration in the combustion region and residence time of combustion gas in the high temperature region, affect the thermal NO formation. From the results seen earlier, the propane gives higher maximum flame temperature compared to the methane and thus a higher thermal NO formation results. As seen in Fig. 6, the flame length is longer for the propane than the methane and therefore the residence time of the combustion gases is longer for the propane. A longer residence time means a higher thermal NO formation.

4. Conclusions

The laminar flamelet model has been successfully incorporated in a finite volume method and applied to predict combustion characteristics of a turbulent jet flame in a crossflow of highly preheated diluted air. For accurate prediction of NO formation, the unsteady flamelets are calculated by solving the Eulerian particle transport equations in a postprocessing mode. The effects of different diluents and fuels are compared. The carbon dioxide is more effective than the nitrogen in reducing the maximum temperature and NO formation. When the oxygen concentration is high, the maximum flame temperature between the methane and propane at each horizontal cross-section shows a large difference in the downstream. If the oxygen concentration is lowered to 4%, however, nearly the same maximum temperature levels between the two fuels are maintained at each horizontal cross-section. The NO emission indices for two different fuels differ greatly when the oxygen concentration is high. The higher flame temperature together with the longer residence time of the combustion gases for the propane flame in the high temperature region may have attributed to the higher thermal NO formation.

Acknowledgement

This work was supported by KOSEF through the Combustion Engineering Research Center.

References

[1] T. Hasegawa, R. Tanaka, T. Niioka, Combustion with high temperature low oxygen air in regenerative burners, in: Proc. of the First Asia-Pacific Conf. on Combust., Osaka U., Osaka, Japan, May 12–15, 1997. pp. 290–293.

[2] A.K. Gupta, S. Bolz, T. Hasegawa, Effect of air preheated temperature and oxygen concentration on flame structure and emission, J. Energy Resour. Technol. 121 (1999) 209–216.

[3] S. Lille, W. Blasiak, M. Jewartowski, Experimental study of the fuel jet combustion in high temperature and low oxygen content exhaust gases, Energy 30 (2005) 373–384.

[4] M. Mortberg, W. Blasiak, A.K. Gupta, Combustion of normal and low calorific fuel in high temperature and oxygen deficient environment, Combust. Sci. Technol. 178 (2006) 1345–1372.

[5] J. Yuan, I. Naruse, Modeling of combustion characteristics and NO_x emission in highly preheated and diluted air combustion, Int. J. Energy Res. 22 (1998) 1217–1243.

[6] S. Orsino, R. Weber, Numerical simulation of combustion of natural gas with high-temperature air, Combust. Sci. Technol. 170 (2001) 1–34.

[7] W. Yang, W. Blasiak, Numerical study of fuel temperature influence on single gas jet combustion in highly preheated and oxygen deficient air, Energy 30 (2005) 385–398.

[8] N. Peters, Laminar diffusion flamelet models in non-premixed turbulent combustion, Prog. Energy Combust. Sci. 10 (1984) 319–339.

[9] H. Pitsch, M. Chen, N. Peters, Unsteady flamelet modeling of turbulent hydrogen–air diffusion flames, Proc. Combust. Inst. 27 (1998) 1057–1064.

[10] H. Barths, N. Peters, N. Brehm, A. Mack, M. Pfitzner, V. Smiljanovski, Simulation of pollutant formation in gas-turbine combustion using unsteady flamelets, Proc. Combust. Inst. 27 (1998) 1841–1847.

[11] P.J. Coelho, N. Peters, Unsteady modeling of a piloted methane/air jet flame based on the Eulerian particle model, Combust. Flame 124 (2001) 444–465.

[12] P.J. Coelho, N. Peters, Numerical simulation of a mild combustion burner, Combust. Flame 124 (2001) 503–518.

[13] K.W. Lee, D.H. Choi, Prediction of NO in turbulent diffusion flames using Eulerian particle flamelet model, Combust. Theor. Model. 12 (2008) 905–927.

[14] B. Marracino, D. Lentini, Radiation modeling in non-luminous nonpremixed turbulent flames, Combust. Sci. Technol. 128 (1997) 23–48.

[15] T. Fujimori, D. Riechelmann, J. Sato, Effect of liftoff on NO_x emission of turbulent jet flame in high-temperature coflowing air, Proc. Combust. Inst. 27 (1998) 1149–1155.

[16] K.W. Lee, D.H. Choi, Analysis of NO formation in high temperature diluted air combustion in a coaxial jet flame using an unsteady flamelet model, Int. J. Heat Mass Transfer 52 (2009) 1412–1420.

[17] B.B. Dally, A.R. Masri, R.S. Barlow, G.J. Fiechtner, Instantaneous and mean compositional structure of bluff-body stabilized nonpremixed flames, Combust. Flame 114 (1998) 119–148.

[18] S.H. Smith, M.G. Mungal, Mixing, structure and scaling of the jet in crossflow, J. Fluid Mech. 357 (1998) 83–122.

[19] E.F. Hasselbrink Jr., M.G. Mungal, Transverse jets and jet flames. Part 1. Scaling laws for strong transverse jets, J. Fluid Mech. 443 (2001) 1–25.

[20] E.F. Hasselbrink Jr., M.G. Mungal, Transverse jets and jet flames, Part 2, Velocity and OH field imaging, J. Fluid Mech. 443 (2001) 27–68.

[21] Available from: <http://maeweb.ucsd.edu/~comubstion/cermech>.

[22] J.C. Hewson, Pollutant emissions from nonpremixed hydrocarbon flames, Ph.D. Thesis, UC San Diego, 1997.

[23] R.J. Kee, F.M. Rupley, J.A. Miller, Chemkin-II: a Fortran chemical kinetics package for the analysis of gas-phase chemical kinetics, Sandia Natl. Lab. Rept. SAND89-8009.

[24] R.J. Kee, J. Warnatz, J.A. Miller, A Fortran computer code package for the evaluation of gas-phase viscosities, conductivities and diffusion coefficients, Sandia Natl. Lab. Rept. SAND83-8209.